

An Experimental Study of Combustor Exit Profile Shapes on Endwall Heat Transfer in High Pressure Turbine Vanes

M. D. Barringer

K. A. Thole

Department of Mechanical and Nuclear
Engineering,
Pennsylvania State University,
University Park, PA 16802

M. D. Polanka

Turbines Branch,
Turbine Engine Division,
Air Force Research Laboratory,
WPAFB, OH 45433

The design and development of current and future gas turbine engines for aircraft propulsion have focused on operating the high pressure turbine at increasingly elevated temperatures and pressures. The drive toward thermal operating conditions near theoretical stoichiometric limits as well as increasingly stringent requirements on reducing harmful emissions both equate to the temperature profiles exiting combustors and entering turbines becoming less peaked than in the past. This drive has placed emphasis on determining how different types of inlet temperature and pressure profiles affect the first stage airfoil endwalls. The goal of the current study was to investigate how different radial profiles of temperature and pressure affect the heat transfer along the vane endwall in a high pressure turbine. Testing was performed in the Turbine Research Facility located at the Air Force Research Laboratory using an inlet profile generator. Results indicate that the convection heat transfer coefficients are influenced by both the inlet pressure profile shape and the location along the endwall. The heat transfer driving temperature for inlet profiles that are nonuniform in temperature is also discussed.

[DOI: 10.1115/1.2950072]

Introduction

The performance and durability of the hot section within gas turbine engines are critical operational issues that present many design and research challenges. The hot section of these engines includes both the combustion chamber and the high pressure turbine, the latter of which includes the endwall regions under investigation in this study. Considering that the hot gas temperatures are well above the melting point of the metal turbine hardware, the heat transfer to and aerodynamic loading of these platform regions is of great interest to engine designers. Long exposure to these elevated temperatures can result in the hardware experiencing thermal and mechanical fatigue, which can be better managed if the true turbine inlet conditions are well known and understood.

The spatial profiles of pressure and temperature that exit the combustor and enter the high pressure turbine play an important role in the operation of the engine. These profiles can be nearly uniform or can possess significant gradients near the inner and outer diameter endwalls. Some inlet pressure profiles have relatively high total pressure near the endwall compared to midspan, and some have relatively low total pressure near the endwall compared to midspan. As the flow passes through the turbine passages, these inlet pressure profiles can result in flow migration from the endwall toward midspan or from midspan toward the endwall. From a heat transfer perspective, the critical issue then is what part of the flow field affects a given region on the endwall or airfoil surface, and how does this influence change based on the inlet profiles.

The radial shape of a typical turbulent boundary layer profile has decreasing total pressure from midspan to the endwall. This turbulent boundary layer profile has often been used as an inlet condition in designing turbine vane and blade hardware. The be-

havior and influence, however, of more realistic inlet profile shapes need to be examined in the endwall region. The primary research objective for this paper was to investigate how different radial profiles of temperature and pressure affect the heat transfer along the vane endwall in a high pressure turbine. Testing was performed in the Turbine Research Facility (TRF) located at the Air Force Research Laboratory (AFRL) using a turbine inlet profile generator.

Review of Relevant Literature

Within the recent past, turbine design has focused on incorporating strategically placed cooling holes and slots that serve to directly reduce the heat transfer in certain regions along airfoil surfaces and their endwalls. In addition, contouring the shape of the junction that joins the vanes to the endwalls was performed in studies by Zess and Thole [1] and Lethander et al. [2] to reduce the intensity of secondary flow circulation patterns that take place within the vane passage. Hermanson and Thole [3] showed that these secondary flows can redirect warmer fluid near the midspan toward the endwall and can redirect the cooling flow along the endwall toward midspan, which in turn reduces the benefit of the coolant.

There have been a large number of experimental and computational studies that have focused on turbine vane and blade endwall aerodynamics and heat transfer. Early work performed by Munk and Prim [4], Lakshminarayana [5], and Langston [6] focused on improving the understanding of the secondary flow patterns that develop within airfoil turning passages. It was shown that an inlet flow field consistent with a turbulent boundary layer resulted in the production of secondary flows, which have a direct impact on the primary passage flow by circulating it toward or away from the endwalls. If the inlet total pressure is uniform, the streamline patterns remain unchanged and the secondary flow vortices do not develop.

Several studies have further investigated the influence of the inlet flow field on the development of these secondary flows and vortices. Computational studies by Hermanson and Thole [3]

Contributed by the International Gas Turbine Institute of ASME for publication in the JOURNAL OF TURBOMACHINERY. Manuscript received July 26, 2007; final manuscript received December 5, 2007; published online January 23, 2009. Review conducted by David Wisler. Paper presented at the ASME Turbo Expo 2007: Land, Sea and Air (GT2007), Montreal, Quebec, Canada, May 14–17, 2007.

showed that the total pressure field is the driving force in the development of secondary flows and heat transfer present in turbine vane passages. They also reported that a counter-rotating vortex (CRV) can exist, in addition to the passage vortex (PV), within the vane passage that can drive fluid away from the endwall and toward midspan. This counter-rotating vortex was found for an inlet total pressure profile containing a positive inflection point (IP) in the spanwise direction near the endwall. Colban et al. [7,8] experimentally confirmed the existence of this counter-rotating PV by studying the effects of varying the film cooling flow through the liner and exit junction slot in a large-scale combustor simulator. Their study documented the passage secondary flow vectors for different vane inlet total pressure profiles and reported a counter-rotating vortex located above the PV for a vane inlet pressure profile containing a positive IP near the endwall.

Kost and Nicklas [9] also found that coolant injected along the vane endwall significantly affected the secondary flow development by strengthening the formation of the leading edge horseshoe vortex (HSV). The increased vortex strength depended on the axial location of the injection with respect to the leading edge stagnation point. They also found that coolant injected through an upstream slot and endwall film cooling holes acted to reduce the endwall cross flow (ECF) and PV by altering the endwall boundary layer thickness. In a study by Kang et al. [10] it was found that a relatively high vane exit Reynolds number ($Re=1.2 \times 10^6$) resulted in the vane PV lifting off the endwall and onto the vane suction surface. The same result was not found for a lower exit Reynolds number ($Re=6.0 \times 10^5$). The vortex lift-off resulted in a decrease in the endwall static pressure, thus causing a different surface heat transfer pattern compared to the lower exit Reynolds number. The high Reynolds number case resulted in the peak heat transfer occurring near the suction surface endwall interface, but for the low Reynolds number the peak occurred more toward midpassage. The separation of the boundary layer occurred farther upstream of the stagnation point for the high Reynolds number case.

The vane passage secondary flow development and endwall heat transfer were also found to be influenced by high freestream turbulence in a study by Radomsky and Thole [11]. They reported a region of high heat transfer upstream of the vane stagnation point corresponding to the formation of the HSV. The center of this HSV was found to be physically closer to the vane surface for high freestream turbulence (19.5%) compared to low freestream turbulence (0.6%). The difference in location was attributed to the elevated turbulence increasing the near wall approach velocities resulting in the vortex being pushed closer to the vane. Within the vane passage, relatively high Stanton numbers were found near the suction surface, while further downstream within the passage the Stanton numbers became aligned with the flow direction. Elevated freestream turbulence levels were found to increase the heat transfer over the entire endwall, with the exception of near the trailing edge where there was little reported augmentation. They reported that the secondary flows dominated the heat transfer near the trailing edge rather than freestream turbulence.

Blair [12] reported that secondary flows direct coolant along the vane endwall across the channel from the pressure surface toward the suction surface. This cross-passage pressure gradient results in increased cooling near the vane-endwall junction along the suction side and reduced cooling near the vane-endwall junction along the pressure side. The extent of the endwall cooling increased somewhat with increased coolant mass flow. Data recorded near the pressure surface showed a more rapid decrease in the film effectiveness compared to the midpassage. With no upstream coolant injection, the heat transfer was greater near the leading edges of both the suction and pressure surfaces than in the midpassage region. This increase in heat transfer was attributed to the leading edge vortex distorting the endwall boundary layer.

Haldeman and Dunn [13] performed heat transfer measurements in a full stage high pressure turbine. For the vane inner

endwall, the results showed that the Stanton number increased significantly through the passage with increasing axial chord. In the pitch direction, the magnitude of the heat transfer was highest for gauge locations nearest to the pressure and suction surfaces compared to gauges located near midpassage. They also reported that the vane-endwall Stanton numbers were in a similar elevated range as the airfoil itself. Similar results were found by Povey et al. [14] who studied the effects of radial inlet temperature distortion on vane and endwall heat transfer in a high pressure turbine facility. Their results also showed that the endwall Nusselt numbers increased with increasing distance within the passage. They also reported similar elevated Nusselt numbers along the endwall as the vane surface. They reported a large decrease in heat transfer along the hub and casing endwalls with inlet temperature distortion compared to an inlet temperature profile that was nearly uniform. The decrease in Nusselt number along the midpassage hub endwall was between 30% and 50%, while along the midpassage casing endwall it was between 25% and 35%. This reduction in heat transfer was attributed to lower local total temperatures of the flow near the endwalls rather than a decrease in the heat transfer coefficient. They found that this reduction in heat transfer was similar for two different circumferential clocking positions of a hot streak, which suggested that the relative circumferential position of the hot streak and vane did not affect the endwall heat transfer.

A study by Nicklas [15] reported that the front part of a transonic turbine vane passage without endwall film cooling experiences relatively constant levels of heat transfer coefficients. Graziani et al. [16] found similar results for the inlet region of a large-scale blade endwall. They reported that the area of influence of the HSV is larger for a relatively thicker inlet boundary layer. They reported elevated heat transfer along the endwall near the airfoil leading edge as well as similar minimum and maximum Stanton numbers for the thick and thin inlet boundary layers. The lowest values of Stanton number were reported near the pressure surface for both inlet boundary layers. The highest values of heat transfer on the endwall were found in the blade wake region for both inlet boundary layer types.

There are relatively few studies in the current literature that have investigated the effects of different realistic inlet temperature and pressure profiles on vane-endwall heat transfer. The temperature profiles exiting combustors and entering turbines become less peaked than in the past and become more spatially uniform. This trend is primarily due to operating the engine hot section closer and closer to its stoichiometric theoretical limits. As the combustor exit thermal fields become more uniform, the hot mainstream gases are in closer proximity to the vane-endwall regions. This has placed great emphasis on the need for a better understanding of how different types of inlet temperature and pressure profiles affect the flow and thermal migration within the first stage turbine passages, especially near the endwalls. The goal of the current study is to examine several different turbine inlet profiles and their corresponding endwall heat transfer levels.

Test Facility and Instrumentation

All testing in the current study was performed at the TRF, which is located in the AFRL at Wright Patterson Air Force Base. This facility operates in a short duration blowdown manner in which several aerothermal engine parameters are matched. These nondimensional parameters include Reynolds number, Mach number, pressure ratio, gas to metal temperature ratio, and corrected mass flow. A photograph of the facility is shown in Fig. 1 and it consists primarily of a large supply tank, a turbine test section, and two large vacuum tanks. The facility has been fully documented by Haldeman et al. [17].

The nitrogen gas working fluid is pressurized and heated within the supply tank prior to testing and the turbine section and vacuum tanks are evacuated. Testing then begins by activating the supply tank main valve, at which time the gas flows through the



Fig. 1 Photograph of the TRF facility

turbine test section and into the vacuum tanks. The mass flow rate is set by controlling the turbine pressure ratio using a variable area isolation valve located downstream of the main test section. The duration of the tests in the current study was approximately 5 s, which was dependent on the size of the turbine being tested. Due to the short test duration, all instrumentation measurements were recorded simultaneously in real time onto data storage units. The data were simultaneously acquired across 200 12 bit channels having a maximum frequency response of 100 kHz and 200 16 bit channels having a maximum frequency response of 200 kHz. Signal conditioning on each channel was performed using low pass filters and built-in amplifiers. All data reduction was performed at a later time.

The turbine test section is a true scale, fully annular, half turbine stage and for this particular study, it was operated in a vane only configuration, as shown in the facility drawing in Fig. 2. The turbine inlet profile generator, documented by Barringer et al. [18], was used in the current study to allow turbine testing to be performed with inlet profiles of pressure and temperature representative of those exiting engine combustors including realistic turbulence intensities and length scales. Several different radial and some circumferential profiles of temperature and pressure were obtained from General Electric, Pratt & Whitney Engines, and the Air Force Research Laboratory during the design phase of the inlet profile generator. These engine profile data in conjunction with several combustor simulator exit pressure profiles docu-

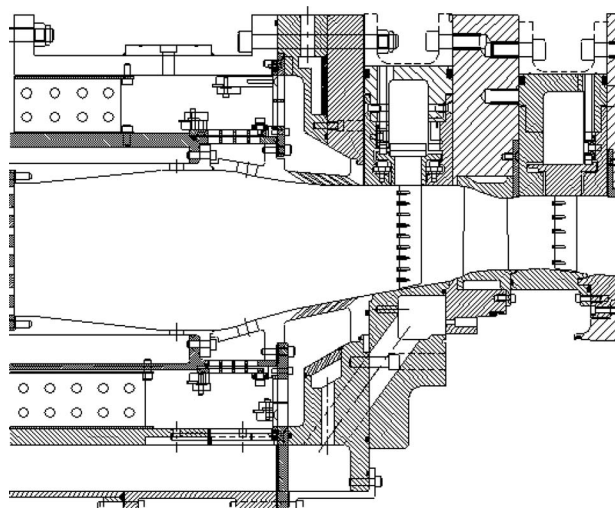


Fig. 2 Drawing of the TRF test rig in a vane only configuration with the inlet profile generator



Fig. 3 Photograph of the turbine vane OD endwall instrumented with thin film heat flux gauges

mented by Colban et al. [7,8] were studied to help determine the proper radial profile shapes that the simulator should be capable of producing.

The inlet profile generator can also be seen in Fig. 2 upstream of the test vane ring. The generator operates by mimicking an aeroengine combustor in which it injects several different flow streams at different temperatures into a central chamber via dilution holes and film cooling holes. The injection flow rates, momentum flux ratios, and temperatures of the different flow streams are varied depending on the desired turbine inlet profile shapes.

The turbine inlet and exit profiles were measured using several instrumentation rakes located on traverse rings upstream and downstream of the turbine section. The rakes contain multiple thermocouples or multiple pressure transducers that are spaced to obtain measurements over equal annular flow areas. The tests discussed in this study involved circumferentially traversing these rakes by approximately 90 deg during the blowdown to obtain both radial and circumferential data. For the turbine inlet profiles being analyzed in the current study a temperature rake was used that contained seven 0.0254 mm diameter thermocouple beads with a thermal time constant of approximately 1.1 ms. Two pressure rakes were also used each containing nine miniature high frequency pressure transducers. All flow and thermal measurements were sampled at 20 kHz. The heat flux along the outer diameter (OD) endwall was measured using Oxford thin film heat flux gauges [19]. Heat flux measurements were not taken along the inner diameter (ID) endwall. The layout of the individual gauges can be seen in the photograph in Fig. 3. Seven gauges were placed near the vane passage inlet, along the pressure side of the vanes, and near the passage exit, as shown in the schematic in Fig. 4.

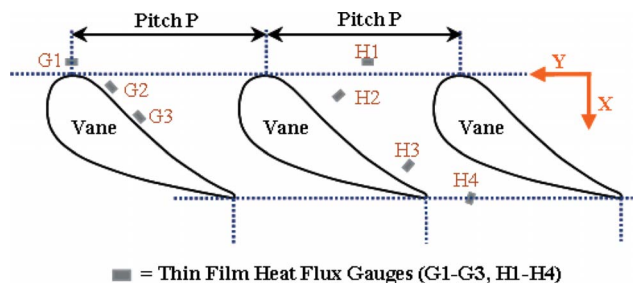


Fig. 4 Schematic of the OD endwall indicating the locations of the thin film heat flux gauges

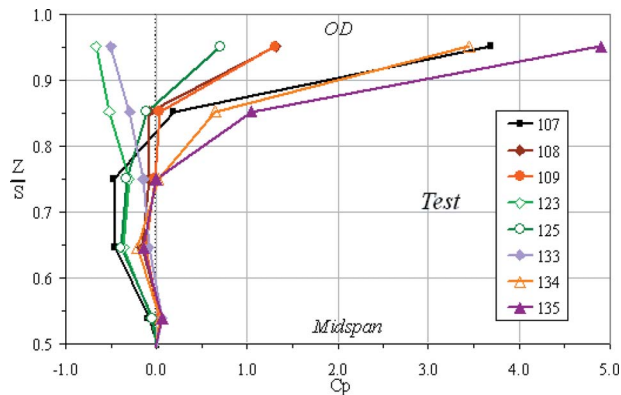


Fig. 5 Radial total pressure profiles measured at the vane inlet near the OD

Based on the uncertainties in the measurement of the heat flux gauge resistance and the uncertainty in calibration from resistance to temperature, the surface temperature uncertainty for the heat flux measurement was calculated to be ± 0.8 K for the heat flux gauges. A jitter analysis, described by Moffat [20], was then performed through the reduction scheme to obtain the uncertainty in the surface heat flux. This resulted in uncertainties in heat flux up to 2000 W/m^2 depending on the gauge. The uncertainty in flow temperature is approximately 0.7 K. The uncertainty in the end-wall heat transfer coefficient was determined to be approximately $30 \text{ W/m}^2 \text{ K}$ for the thin film gauges based on uniform inlet temperature profiles. This corresponded to Nusselt number uncertainties between 5% and 9% depending on location. The uncertainty in the endwall heat transfer coefficient for nonuniform inlet temperature profiles is discussed in the following sections.

Vane Inlet Conditions

The pressure and temperature profiles that are analyzed in this study were generated during a series of tests whose flow conditions are reported in more detail by Barringer et al. [18]. To summarize the test conditions, the flow at the turbine inlet for all of the profiles presented in this study corresponds to a mean Reynolds number of $\text{Re}=2.1 \times 10^5$ and a mean axial Mach number of $M=0.1$. The turbulence intensity associated with these turbine inlet profiles was found to be in an elevated range between $\text{Tu}=20\text{--}30\%$. The longitudinal integral length scale was found to be near 30% of the vane pitch, which corresponds to 2.3 times the vane leading edge diameter.

Several radial total pressure profiles at the turbine vane inlet are shown in Fig. 5 from midspan ($Z/S=0.5$) to the OD endwall ($Z/S=1.0$). The profiles are plotted in terms of a normalized total pressure coefficient C_p defined as the local total pressure subtracted by the midspan total pressure all divided by the average dynamic pressure at the vane inlet. Note that by this definition $C_p=0$ at midspan. These radial profiles have been circumferentially (spatially) averaged across one full vane pitch along lines of constant radius that are spaced at equal annular flow areas and represent the mean vane inlet conditions. The test numbers are a numeric record of the facility settings used within the inlet profile generator and supply tank. These settings were summarized in tabular form by Barringer et al. [18] for each test number. Each test is different since the inlet profile generator settings are different for each test. The settings within the inlet profile generator control the mass flow rate and temperature of the film cooling flow, dilution flow, and core mainstream flow. These different settings result in different pressure and temperature profile shapes entering the vanes.

A range of pressure profile shapes can be seen including some that contain sharp gradients near the OD endwall in Fig. 5. These

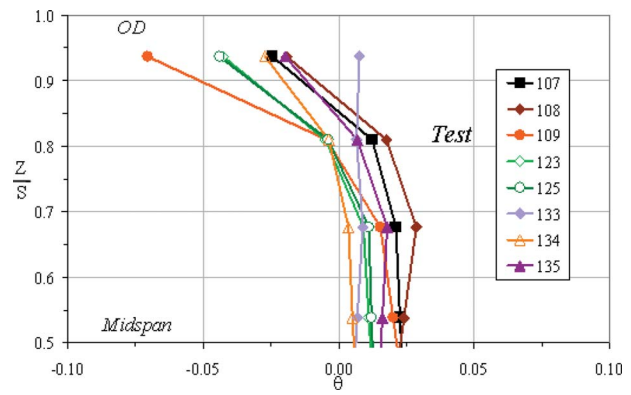


Fig. 6 Radial total temperature profiles corresponding to the pressure profiles in Fig. 5

gradients are the result of varying amounts of upstream film coolant being injected into the mainstream flow along the endwall. The C_p values near the OD endwalls at $Z/S=0.95$ were found to be directly related to the upstream film cooling momentum flux ratio where an increase in this ratio resulted in an increase in the maximum C_p value [18]. It is important to note that a negative C_p value does not mean that the flow is in the reverse upstream direction; it simply means that the local total pressure is less than that at the midspan. This behavior can be seen for Tests 123 and 133, which possess slightly less total pressure near the OD endwall (compared to the midspan). This profile behavior is characteristic of a turbulent boundary layer in that the total pressure decreases with increasing proximity to the endwall. This is in contrast to the pressure profiles for Tests 107, 108, 109, 125, 134, and 135; all of which are characterized by positive C_p values at $Z/S=0.95$ indicating that an increase in total pressure takes place near the endwall. It is expected that all of these pressure profile shapes exhibit a similar trend closer to the endwall in which a negative gradient should be present.

The radial total temperature profiles at the turbine vane inlet corresponding to the total pressure profiles in Fig. 5 are shown in Fig. 6. The temperature profiles are plotted in terms of a nondimensional total temperature coefficient θ defined in the Nomenclature. These radial temperature profiles have also been circumferentially averaged across one full vane pitch along lines of constant radius that are spaced at equal annular flow areas. It can be seen that one of the temperature profiles is nearly uniform in the radial direction from midspan to the OD endwall, Test 133. The remaining thermal profiles, however, contain moderate to significant gradients near the endwall. These endwall gradients were found to scale with the upstream film cooling momentum flux ratio and the film coolant temperature [18]. The shapes of the pressure and temperature profiles near midspan are more uniform than near the endwall, which is a result of the intense mixing of the dilution flow in the upstream inlet profile generator.

Secondary Flow Patterns

There are several means by which the inlet total pressure profile can alter the vane-endwall heat transfer. It can change the local boundary layer thickness and turbulence intensity. The inlet pressure profile can also affect the secondary flow vorticity (rotation direction), turnover rate, vortex size, and vortex trajectory. All of these physical mechanisms influence the convective heat transfer coefficients along the endwall.

The different total pressure profiles at the vane inlet result in different secondary flow development within the vane passage. The HSV that forms at the vane leading edge junction will have a range of flow circulation patterns within the vane passage depending on whether the inlet total pressure profile near the endwall is consistent with a typical turbulent boundary layer ($C_p < 0$), has

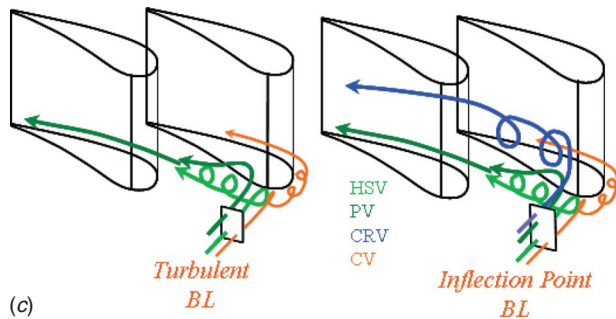
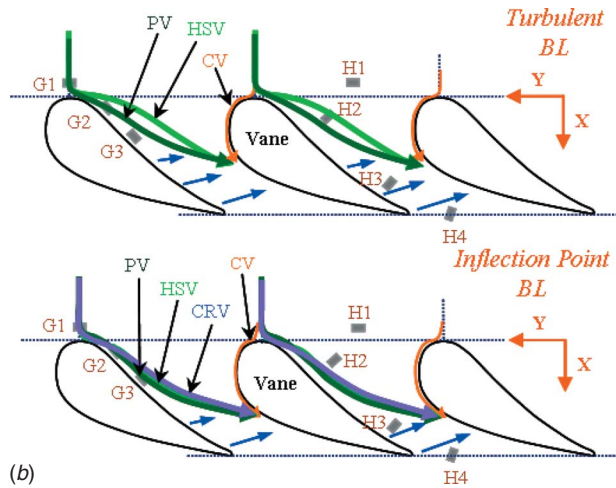
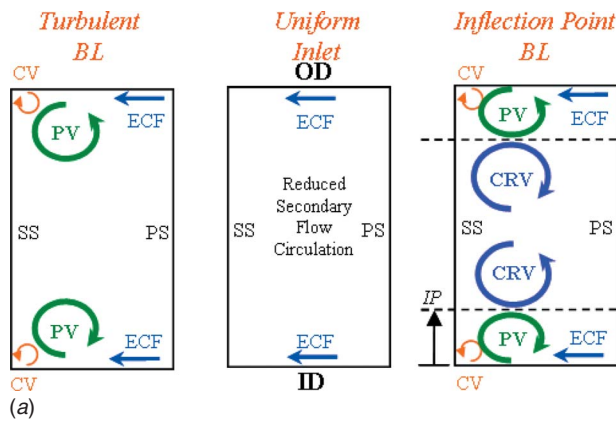


Fig. 7 Schematics illustrating secondary flow patterns that develop within the vane passage including (a) a cross-passage view near midaxial chord looking downstream, (b) a span view looking toward the endwall, and (c) an isometric view upstream looking downstream

nearly uniform pressure ($C_p \approx 0$), or contains a forward facing IP ($C_p > 0$). The schematic shown in Fig. 7(a) illustrates the different circulation patterns within the vane passage near midaxial chord for these three pressure profile scenarios.

For the turbulent boundary layer scenario ($C_p < 0$), a PV and suction side corner vortex (CV) form near the endwalls circulating mainstream flow and ECF along the endwall toward the suction side of the vane. The PV is considerably larger than the CV and also directs flow from the endwall toward the midspan. For the near uniform inlet condition scenario ($C_p \approx 0$) with near uniform total pressure, there is no significant secondary flow pattern present within the vane passage. For the inlet boundary layer scenario with an IP in total pressure ($C_p > 0$), the PV and CV will

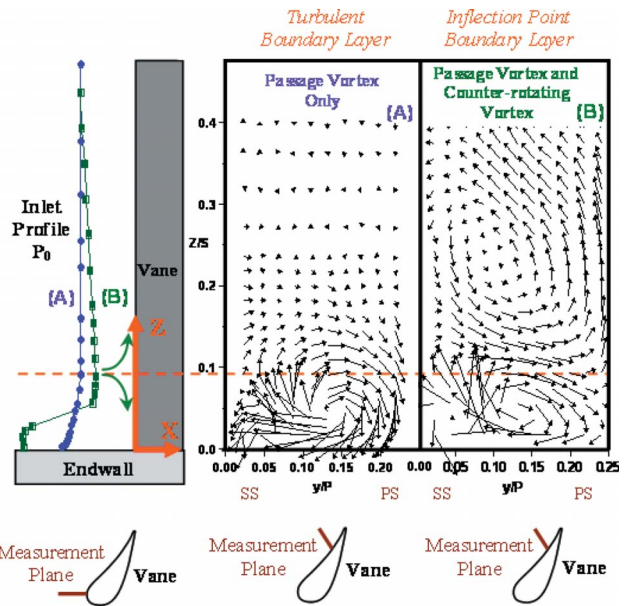


Fig. 8 Velocity contours within the vane passage ($X/C=0.35$) from Colban et al. [8] showing secondary flow vectors and their corresponding vane inlet total pressure profiles for (a) a turbulent boundary layer and (b) a forward facing IP boundary layer near the endwall

form as well as a CRV, which is larger in size than the PV. The CRV develops in this case since the inlet total pressure profile has an IP that is located near the endwall, typically somewhere between 0% and 15% of the vane span. The span location where the PV and CRV become tangent corresponds to the general span location of the IP.

The schematics shown in Figs. 7(b) and 7(c) show conceptually that when the total pressure near the endwall at the vane inlet is less than the midspan total pressure, then the near endwall flow field contains both (1) the HSV that develops near the vane leading edge and (2) the PV that forms from fluid entering the vane inlet that passes over top of the HSV and then down into the relatively lower pressure region along the endwall behind the HSV. The pressure side portion of the HSV combines with this PV into one vortex near midaxial chord, and then finally this combined PV crosses over the passage toward the suction side of the adjacent vane where it continues until it reaches the vane passage exit. The suction side portion of the HSV remains relatively small and close to the suction side endwall junction where it is eventually overcome by the PV. Note that in Fig. 7(a), the passage vortex that is shown refers to the combined PV. When the total pressure near the endwall at the vane inlet is larger than the midspan total pressure and contains an IP near the endwall, then the near endwall flow field contains (1) and (2) just described but also contains the CRV. The CRV develops from fluid entering the vane that is above the IP and rotates in an opposite direction compared to the combined PV.

The concepts that are illustrated in Fig. 7 were developed based on the findings from both Hermanson and Thole [3] and Colban et al. [8]. Experimental data from the study of Colban et al. [8] are shown in Fig. 8 including example secondary flow vectors within the vane passage for two different types of vane inlet pressure profiles. Their study confirmed the presence of a counter-rotating vortex located above the PV when the vane inlet pressure profile contains a slight forward facing IP near the endwall. This is illustrated in Fig. 8, which shows secondary flow vectors within the vane passage at approximately $X/C=0.35$. The turbulent bound-

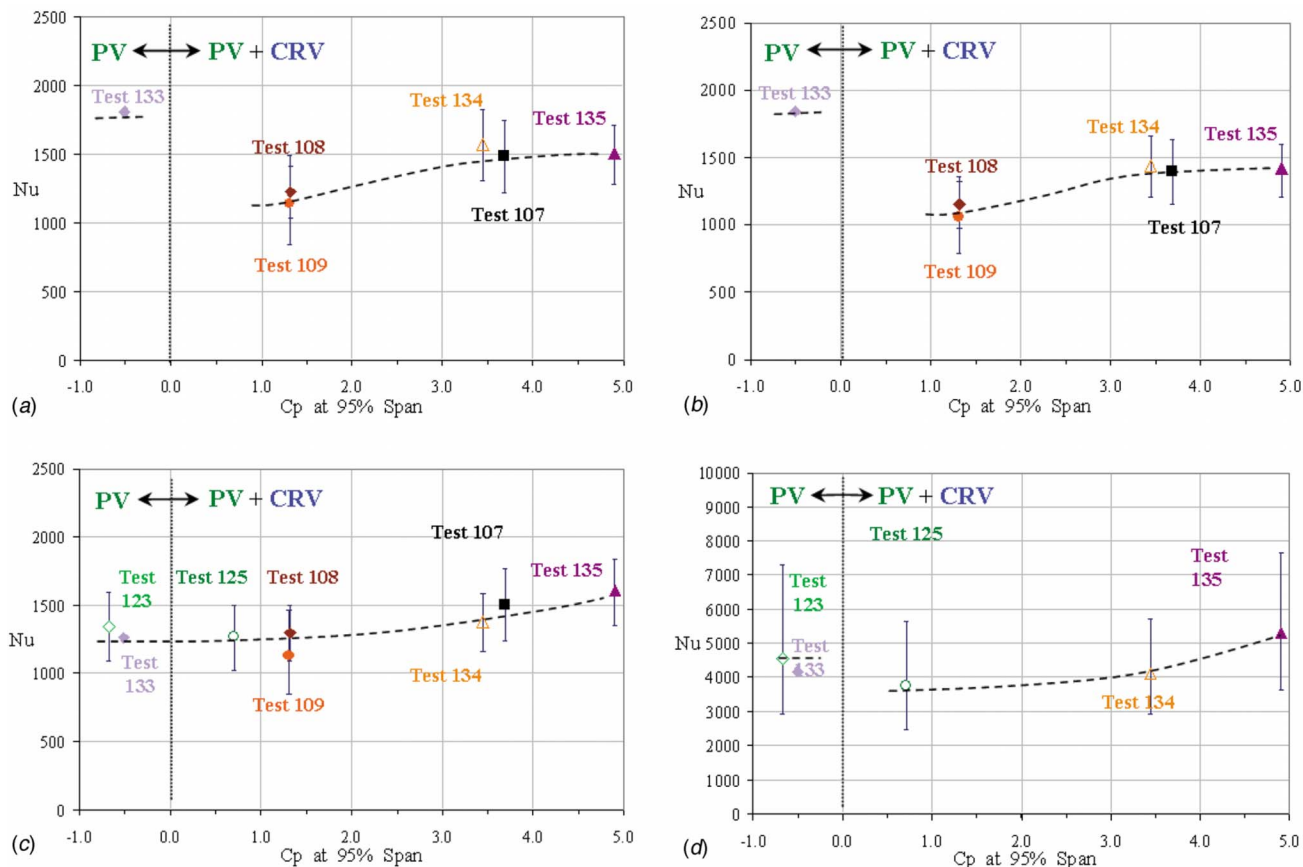


Fig. 9 Nusselt number scaling for heat flux gauge (a) G1 near vane stagnation, (b) G2 near the vane pressure side leading edge, (c) H1 at the passage inlet near midpitch, and (d) H2 near the passage inlet near midpitch

ary layer profile has lower total pressure near the endwall relative to midspan, and the IP profile has higher total pressure near the endwall at $Z/S=0.1$ relative to midspan.

The inlet total temperature profile can also alter the vane-endwall heat transfer. Inlet temperature profiles that are nearly uniform in shape result in fluid temperatures near the endwall that are very similar to the hot midspan flow, which results in increased wall temperatures. Inlet temperature profiles with negative thermal gradients near the endwall have fluid temperatures near the wall that are cooler than the hot midspan flow, which results in reduced endwall metal temperatures for the same convection coefficient. Depending on the corresponding inlet pressure profile shape, the fluid near the wall can be circulated toward midspan or the fluid near midspan can be circulated toward the endwall.

Endwall Heat Transfer Measurements

The heat transfer measurements taken on the OD endwall are reported in this section for the different inlet profiles shown in Figs. 5 and 6. The heat transfer for each of the seven heat flux gauges is documented in Figs. 9 and 10 in the form of Nusselt number, which is defined in the Nomenclature. The convective heat transfer coefficient was obtained by dividing the measured heat flux by an appropriate driving temperature. The driving temperature associated with the local heat flux was defined as the difference between the measured wall surface temperature (T_w) and the total temperature of the freestream (T_∞) in the vicinity of the heat flux gauge, which is now discussed.

The issue of how to determine T_∞ near the individual heat flux gauges is a challenging problem since detailed flow and thermal field data within the vane passage could not be taken for the various inlet profiles. Simply using the mean flow temperature

that enters the turbine vane as a driving temperature for all endwall surface locations and regions has been done in many past studies involving turbine heat transfer but a better approximation of the true driving temperature must be estimated for realistic inlet conditions that are not uniform. It was decided that the mean flow temperature at the vane inlet in the span range $0.75 < Z/S < 1.0$ was a more accurate definition for T_∞ since the flow field in this span region significantly affects the endwall region. This definition is used consistently for all gauges and for all tests discussed below. However, its applicability is also examined in this section at different locations along the endwall.

For inlet flows where the near endwall total pressure has $C_p < 0$, the PV circulates fluid within approximately 20% of the vane span toward the endwall throughout the passage [21]. Near the leading edge region, when $C_p > 0$ the fluid between the IP span location and endwall is circulated toward the endwall. However, at axial locations within the passage where the edges of the PV and CRV vortices interact with one another, the endwall is not limited to the inlet profile flow temperatures between the endwall and the IP. At these axial locations, the endwall can see temperatures from fluid that originated farther away from the endwall at the vane inlet. For example, the CRV can circulate fluid near midspan toward the IP span location and then the PV can circulate a portion of this same fluid layer toward the endwall. Note, however, that this overall circulation from CRV to PV to endwall would take place over a finite streamwise distance, and this distance may change slightly depending on the size and strength of the vortices. The secondary flow patterns emphasize that the endwall driving temperature is dependent on the location within the passage as well as the inlet pressure and temperature profile shapes.

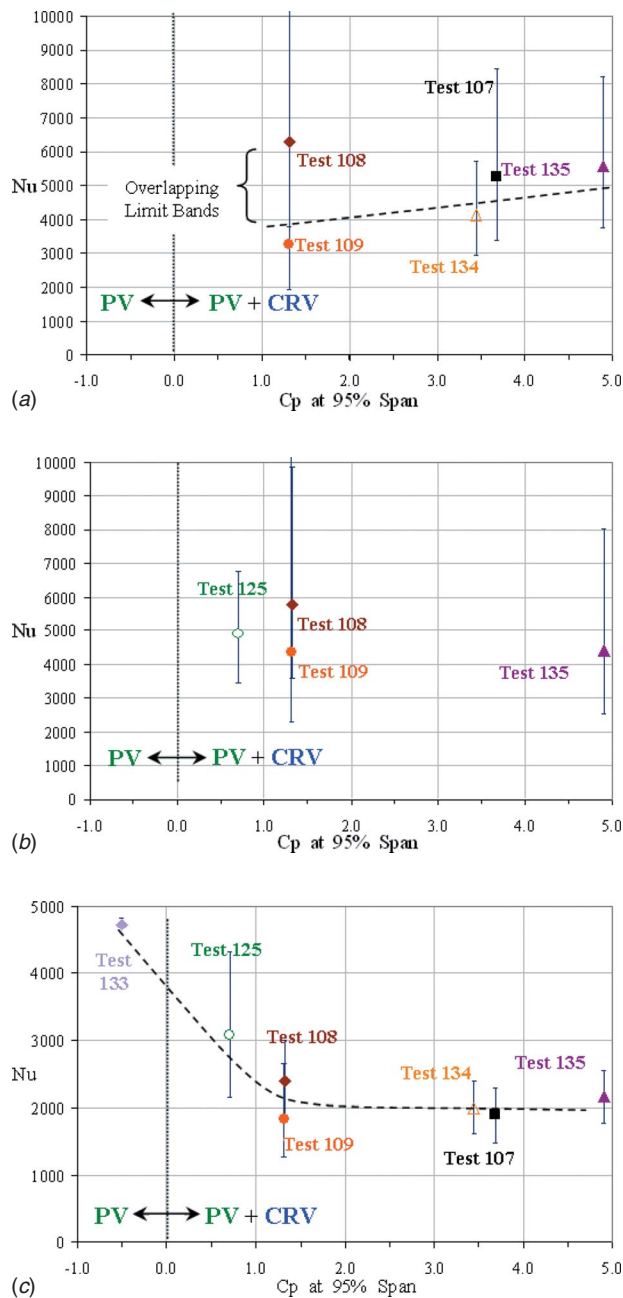


Fig. 10 Nusselt number scaling for heat flux gauge (a) G3 near the vane pressure side at midaxial chord, (b) H3 near the vane pressure side trailing edge, and (c) H4 near the vane passage exit

No matter how T_∞ is defined, the convection heat transfer coefficient h at a given endwall location should be very similar for two inlet pressure profiles that have nearly the same shape and C_p values, as long as they also both have nearly the same inlet Reynolds number and Mach number. In other words, if two different tests have the same inlet C_p value near the endwall, for example, Tests 108 and 109 in which $C_p \approx 1.3$ at $Z/S=0.95$, but one test resulted in $\theta=-0.02$ (Test 108) near the endwall and the other test resulted in $\theta=-0.07$ (Test 109) near the endwall, then the convection coefficient h should be nearly the same value, since h itself is not a function of temperature.

Figures 9(a)–9(d) and 10(a)–10(c) compare the Nusselt number with the C_p value measured at $Z/S=0.95$ near the OD endwall. The available data points that are plotted correspond to the previ-

ously mentioned driving temperature definition for the convective heat transfer coefficients. The plus and minus bands on each data point correspond to the Nusselt number that would occur at the maximum and minimum measured flow temperatures at the vane inlet in the span range $0.75 < Z/S < 1.0$. The plus and minus bands do not represent error bars. The dashed curve represents the general trend in Nusselt number as a function of the C_p value near the endwall. As the inlet total pressure profile near the endwall is changed, the pressure field that drives the local flow also changes, including a change in the secondary flow. This will directly impact the convection heat transfer coefficients near the endwall. The magnitude and sign of the change in h depend on the magnitude of the change in the inlet total pressure and the location within the vane passage.

The heat transfer measurements taken near the vane leading edge stagnation region are shown in Fig. 9(a) for heat flux Gauge G1 that is positioned at $X/C=-0.12$ (see Fig. 4). This location should be close to the position where the HSV begins to form. It can be seen in Fig. 9(a) that the limit bands for Test 133 are very small, which is due to the near uniform temperature profile near the OD for this particular test. It can also be seen that the data points for Tests 108 and 109 are very similar in Nu, which implies that the driving temperature definition mentioned previously is consistent (since the driving temperature value is different for these two test conditions). The fact that Tests 108 and 109 have nearly identical pressure profiles near the OD endwall suggests that very similar convection heat transfer coefficients should be present, and this is the case. Similar h values are also seen for Tests 134 and 107, which have similar C_p values ($C_p \approx 3.5$) at $Z/S=0.95$. The Nu data point for Test 134 is slightly higher than for Test 107 but agreement still occurs within the limit bands.

The results in Figs. 9(a) and 9(b) indicate that the heat transfer coefficient near the vane leading edge stagnation region is higher for an inlet profile with C_p less than but nearly equal to zero, as compared to an inlet profile with $C_p > 0$. Between $-0.5 < C_p < 1.2$ there is a clear reduction in Nu. It is believed that this reduction in Nu is the result of the HSV separation point moving in the axial direction, relative to the vane stagnation point, due to a change in the endwall inlet C_p value. Both Figs. 9(a) and 9(b) show that for inlet profiles with $C_p > 0$, as the total pressure is increased along the OD endwall the value of h increases, which is a result of the velocity increasing in magnitude.

Figure 9(b) shows that the heat transfer results for heat flux Gauge G2 are slightly lower but very similar to G1 (Fig. 9(a)). Heat flux Gauge G2 is positioned near the vane pressure side leading edge at $X/C=0.06$ (see Fig. 4). The evident similarity in heat transfer behavior between Gauges G1 and G2 is due to their close endwall proximity. It is believed that Gauge G2 is only slightly influenced by the edge of the PV and HSV, and therefore the same driving temperature definition is applicable. Again, there is good agreement in the Nusselt number values between Tests 108 and 109 and between Tests 107 and 134.

The results for Gauge H1 located at the passage inlet near midpitch (see Fig. 4) are shown in Fig. 9(c). This gauge location is not significantly affected by the secondary flow development as one would expect. As C_p is increased, the local streamwise velocity near the passage inlet increases and results in a continuous increase in the convection heat transfer coefficient. Another important result is that the magnitudes of the Nusselt numbers for Gauge H1 are comparable to those measured for Gauges G1 and G2, which are also located near the passage inlet. This finding is in agreement with the results reported by Nicklas [13] and Graziani et al. [14] in that the front part of the airfoil passage experiences near constant levels of heat transfer coefficients.

The Nusselt number results for Gauge H2 at $X/C=0.12$ near midpitch (see Fig. 4) are reported in Fig. 9(d). The levels reported for this gauge are three to four times higher than those reported at the passage inlet for Gauges G1, G2, and H1. This increase is attributed in part to flow acceleration from the vane passage inlet

to the gauge location, but it is also attributed to the HSV and PV passing over and circulating fluid into the endwall near the gauge location. The general trend shown for Gauge H2 is similar to that of Gauge H1 in that an increase in the inlet profile C_p results in an increase in h . This similarity is expected. Since the Nusselt numbers for Tests 123 and 133 in Fig. 9(d) are similar, this implies that the originally defined driving temperature is still applicable at this location for $C_p < 0$. For Gauge H2, between $-0.5 < C_p < 0.7$ there is a small reduction in Nu. This reduction is similar to the reduction reported for Gauges G1 and G2 between $-0.5 < C_p < 1.2$ and was attributed to the weakening of the HSV and the PV as the inlet total pressure profile near the endwall approaches uniform conditions (as C_p approaches $C_p = 0.0$).

The heat transfer results for heat flux Gauge G3 within the passage at $X/C = 0.3$ (see Fig. 4) are shown in Fig. 10(a). The Nusselt numbers at this location are also nearly three to four times higher than those measured near the leading edge stagnation region. This increase was again attributed in part to the flow accelerating between the passage inlet and $X/C = 0.3$ but also because of the PV passing near the gauge in which freestream fluid is circulated toward the endwall gauge location. Figure 10(a) shows the available data for this gauge, which corresponds to only inlet pressure profiles with $C_p > 0$ near the endwall. This particular gauge was not operating properly during the other tests. For the available data, it can be seen that the previously mentioned driving temperature definition is not very accurate at this gauge location for the C_p values tested since the Nu values for Tests 108 and 109 ($C_p = 1.3$) as well as those for Tests 107 and 134 ($C_p \approx 3.5$) are considerably different. However, the true Nu values for this set of tests should be within their overlapping bands.

The large limit bands in Figs. 10(a) and 10(b) are a result of the relatively higher heat flux values and higher wall temperatures measured at these two gauge locations. The lower limit band is calculated by using the largest driving temperature, which is between T_w and the maximum fluid temperature at the vane inlet between $0.75 < Z/S < 1.0$. The upper limit band is calculated by using the smallest driving temperature, which is between T_w and the minimum fluid temperature at the vane inlet between $0.75 < Z/S < 1.0$.

The true Nu values for Tests 108 and 109 in Figs. 10(a) and 10(b) as well as for Tests 107 and 134 in Fig. 10(a) may, in fact, never fall within their overlapping bands at this location. This is due to the fact that within the vane passage the PV and CRV vortices complete more than one rotation (turn over cycle) and some of this fluid comes in contact with the lower temperature walls, which can change the true driving temperature to something other than the difference between the measured wall temperature and the average of the inlet temperature profile over a certain span region. This is the reason that it is impossible to know for certain what the true T_∞ is for the gauges downstream of the leading edge region within the passage without having well resolved flow field data within the passage or detailed accurate predictions from computational fluids dynamics (CFD). This also emphasizes how difficult these heat transfer measurements are, but more importantly how difficult it is for the engine designer to estimate the right values and use them in their hardware life prediction tools. Turbine designers must be made aware that this is a key reason why the turbine endwalls can see significant thermal fatigue and melting in real engine hardware. An underestimation of the true driving temperature, which can easily take place as shown by the large limit bands, can cause significant hardware failure.

The fluid that reaches Gauge G3 comes from a span location further away from the endwall than for Gauges G1 and G2. In other words, the part of the vane inlet flow field at a span location consistent with the PV is being directed toward this endwall gauge location (see Fig. 7(c)). The PV essentially circulates warmer fluid into this gauge location. For endwall inlet profiles having $C_p > 0$, as C_p is increased the PV and CRV increase in strength and are pushed somewhat closer to the vane pressure side (closer to G3)

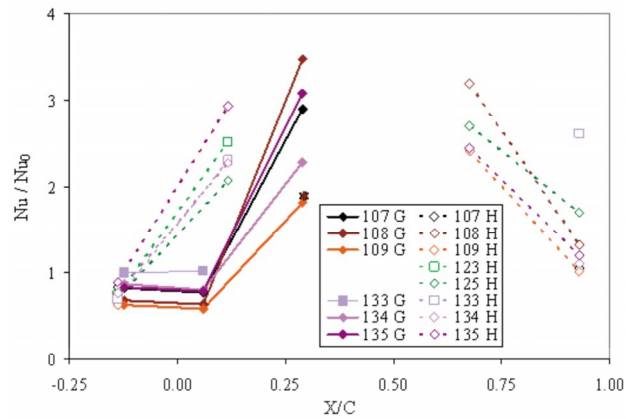


Fig. 11 Nusselt number augmentation versus X/C for each heat flux gauge

prior to crossing the channel to the adjacent vane, which takes place farther downstream within the passage, as was illustrated conceptually in Fig. 7. This results in increased h values near this gauge location.

The Nusselt numbers for Gauge H3 within the passage at $X/C = 0.68$ near midpitch (see Fig. 4) are reported in Fig. 10(b). Gauge H3 experiences the most elevated heat transfer coefficients. This is a result of the gauge being located near the throat of the vane passage and therefore the fluid velocities are relatively high. This gauge location should not be significantly influenced by the secondary flows, and the quantity of available data points shown in Fig. 10(b) is not large enough to draw conclusive comments regarding a trend involving the inlet total pressure profile.

The results for heat flux Gauge H4 near the vane passage exit (see Fig. 4) are shown in Fig. 10(c). In general, this gauge reports that the heat transfer coefficients are larger for inlet profiles with a total pressure coefficient C_p that is less than but nearly equal to zero. It can be seen that as the C_p value is increased, the Nu values decrease and then level out. It is believed that as the inlet total pressure along the OD endwall is increased at the vane inlet, the secondary flow PV trajectory is being shifted away from the heat flux gauge location and thus a reduction in the heat transfer coefficient is observed.

Heat Transfer Augmentation

The OD endwall heat transfer is presented in augmentation form in Fig. 11. The augmentation is with respect to the heat transfer coefficient Nu_0 determined in the endwall stagnation region measured with Gauge G1 for Test 133, which had near uniform inlet temperature and an endwall $C_p = -0.5$ at $Z/S = 0.95$. The data points connected with solid lines and solid symbols correspond to heat flux Gauges G1–G3 that are positioned at a pitch location near the pressure side of the vane upstream of midaxial chord. The data points connected with dashed lines and open symbols correspond to heat flux Gauges H1–H4 that are positioned at a pitch location closer to midpitch and are distributed from the passage inlet to the passage exit.

It can be seen from Fig. 11 that the heat transfer coefficient depends on both the location within the vane passage and the inlet profiles. The augmentation near the passage inlet for a given inlet profile is nearly the same for Gauges G1 and H1 with values ranging from $Nu/Nu_0 = 0.6$ to 1.0 depending on the profile. This helps illustrate that inlet profiles that have a total pressure coefficient C_p value less than but close to zero result in higher endwall heat transfer near the passage inlet than inlet profiles with $C_p > 0$. It can also be seen that this Nu/Nu_0 range is similar for Gauge G2, which is a result of the similar heat transfer behavior between G1 and G2 that was shown in Fig. 9. These three gauges

have Nusselt numbers consistent with the stagnation region Nusselt numbers on the airfoil surface, as reported by Barringer et al. [22].

Downstream of Gauge G2 within the region $0.12 < X/C < 0.68$ the augmentation for Gauges G3, H2, and H3 shows a significant rise in Nu/Nu_0 for both pitch locations. This increase in Nusselt number is due in part to the flow accelerating within the passage but also because of the secondary flow vortices intensifying the local flowfield in the vicinity of the gauges. The Nusselt number in this region is thus the highest experienced within the vane section. It is important to note that since the driving temperature definition was not very accurate for Gauge G3, the data points for Tests 108 and 109 at $X/C=0.3$ should be nearly the same at an augmentation level just below 2.0, as indicated by the star (*) symbol in Fig. 11.

Near the passage exit at $X/C=0.93$, Test 133 resulted in elevated Nusselt numbers similar in magnitude to the other test data shown in Fig. 11 between $0.12 < X/C < 0.68$. However, at $X/C=0.93$ Tests 108, 109, 125, and 134 all resulted in significantly lower augmentation levels than Test 133, and it is interesting that these tests all include inlet pressure profiles with $C_p > 0$. The decrease in augmentation that is seen from $X/C=0.68-0.93$ can be explained by the flow decelerating from the vane passage throat to the passage exit. However, the decrease in augmentation at $X/C=0.93$ between Test 133 and tests 108, 109, 125, and 134 is an indication that as the inlet total pressure along the OD endwall is increased at the vane inlet, the secondary flow PV trajectory is being shifted away from the heat flux gauge location and thus a reduction in the heat transfer coefficient is observed.

An important result from Fig. 11 is that relative to uniform inlet conditions (Test 133) the heat transfer does decrease at the passage inlet and near the passage exit when nonuniform inlet conditions are present at the vane inlet. This finding is consistent with the results from Povey et al. [14]. The uniform inlet conditions result in warmer fluid being near the endwall surface as well as a reduction in secondary flow circulation.

Conclusions

Several different turbine inlet pressure and temperature profiles were investigated to determine their effect on the heat transfer along the OD endwall in a high pressure turbine vane ring. The inlet profiles resulted in a wide range of Nusselt numbers at different locations on the endwall. Near the vane passage inlet as well as the passage exit, the inlet pressure profiles consistent with the shape of a standard turbulent boundary layer resulted in higher Nusselt numbers than inlet profiles with IPs that have higher total pressure near the endwall relative to midspan. At the passage inlet near midpitch, as the total pressure along the endwall was increased a continuous increase in the convection heat transfer coefficient was observed. The endwall gauge locations near the passage inlet near midpitch are more influenced by changes in the inlet Reynolds number than changes in secondary flow patterns.

Some other general trends that were found include relatively uniform heat transfer levels near the passage inlet for both the stagnation and midpitch regions. Along the vane pressure surface the heat transfer levels increase significantly with increasing distance into the passage. The data also showed that near midpitch the rise in heat transfer with increasing distance into the passage occurred closer to the passage inlet compared to further downstream for the gauges located near the pressure side surface of the vane.

For realistic turbine inlet profiles that contain significant gradients near the endwalls in both pressure and temperature, the assumption of a constant freestream temperature throughout the passage as a heat transfer driving mechanism can lead to significant underprediction or overprediction of the true local heat transfer coefficients. The secondary flows that develop near the endwalls vary in strength, size, and trajectory depending on the inlet pressure profile. This results in different driving temperatures for dif-

ferent locations along the endwall, especially in the front half of the passage. However, the secondary flow circulation patterns can be used along with the physical limits of the inlet temperature profile near the endwall as a guide in estimating the true driving temperature and heat transfer trends.

The results from this study are considered useful to turbine engine designers since they show how different inlet profiles affect the convection heat transfer coefficient at several different locations along the OD endwall of a high pressure turbine. The heat transfer trends reported here will allow better design and placement of film cooling holes and slots in the endwall region, both upstream of the vane and within the vane passage since they show the dependency of Nusselt number on the turbine inlet profile and location within the vane passage. This work also emphasizes how difficult this type of heat transfer measurement is, and how challenging it is to predict accurate convection heat transfer coefficients when nonuniform inlet conditions are present. The underprediction of these coefficients and subsequent use in hardware life prediction tools can result in significant thermal fatigue and melting in real engine hardware.

Acknowledgment

The authors would like to thank the AFRL Technology Evaluation Branch for their help in conducting these experiments. The authors would also like to thank Dr. Richard Anthony for the manufacture of the heat flux gauges and Robert Free for installation of the heat flux gauges. The authors would also like to thank the Air Force Research Laboratory at Wright Patterson Air Force Base for funding and sponsoring this research effort.

Nomenclature

C	= specific heat or vane axial chord length
C_p	= pressure coefficient, $C_p = (P_t - P_{t_{ms}}) / \frac{1}{2} \rho_{ave} U_{ave}^2$
h	= convection coefficient, $h = q'' / (T_\infty - T_w)$
k	= thermal conductivity
M	= Mach number
Nu	= Nusselt Number, $Nu = hC / k_f = q''C / (T_\infty - T_w)k_f$
P	= pressure or vane pitch
q''	= heat flux
Re	= Reynolds number, $Re = U_{ave}C / \nu_{ave}$
S	= vane span or total vane surface length
T	= temperature
Tu	= turbulence intensity, $Tu = U_{rms} / U_{ave}$
U	= velocity
X, Y, Z	= axial, pitch, and span directions

Greek

ν	= kinematic viscosity
ρ	= density
θ	= nondimensional temperature, $\theta = (T - T_{ave}) / T_{ave}$

Subscripts

0	= heat flux from Gauge G1 for uniform inlet conditions
∞	= freestream or mainstream
ave	= mean or average conditions
f	= film conditions
MS	= midspan
rms	= root mean square
s	= flow static conditions
t	= flow total conditions
w	= wall surface
x	= axial distance with respect to stagnation

References

- [1] Zess, G., and Thole, K., 1999, "Computational Design and Experimental Evaluation of Using a Leading Edge Fillet on a Gas Turbine Vane," ASME Paper No. 2001-GT-0404.

- [2] Lethander, A., Thole, K., Zess, G., and Wagner, J., 2003, "Optimizing the Vane-Endwall Junction to Reduce Adiabatic Wall Temperatures in a Turbine Vane Passage," ASME Paper No. GT2003-38940.
- [3] Hermanson, K., and Thole, K., 2000, "Effect of Inlet Conditions on Endwall Secondary Flows," *J. Propul. Power*, **16**(2), pp. 286–296.
- [4] Munk, M., and Prim, R. C., 1947, "On the Multiplicity of Steady Gas Flows Having the Same Streamline Pattern," *Proc. Natl. Acad. Sci. U.S.A.*, **33**, pp. 137–141.
- [5] Lakshminarayana, B., 1975, "Effects of Inlet Temperature Gradients on Turbomachinery Performance," *ASME J. Eng. Power*, **97**, pp. 64–74.
- [6] Langston, L. S., 1980, "Crossflows in a Turbine Cascade Passage," *ASME J. Eng. Power*, **102**, pp. 866–874.
- [7] Colban, W. F., Thole, K. A., and Zess, G., 2002, "Combustor-Turbine Interface Studies-Part 1: Endwall Effectiveness Measurements," ASME Paper No. GT2002-30526.
- [8] Colban, W. F., Thole, K. A., and Zess, G., 2002, "Combustor-Turbine Interface Studies-Part 2: Flow and Thermal Field Measurements," ASME Paper No. GT2002-30527.
- [9] Kost, F., and Nicklas, M., 2001, "Film-Cooled Turbine Endwall in a Transonic Flow Field: Part I-Aerodynamic Measurements," ASME Paper No. 2001-GT-0145.
- [10] Kang, M., Kohli, A., and Thole, K. A., 1999, "Heat Transfer and Flowfield Measurements in the Leading Edge Region of a Stator Vane Endwall," *ASME J. Turbomach.*, **121**(3), pp. 558–568.
- [11] Radomsky, R., and Thole, K. A., 2000, "High Freestream Turbulence Effects in the Endwall Leading Edge Region," *ASME J. Turbomach.*, **122**, pp. 699–708.
- [12] Blair, M. F., 1974, "An Experimental Study of Heat Transfer and Film Cooling on Large-Scale Turbine Endwalls," *ASME J. Heat Transfer*, **96**(4), pp. 524–529.
- [13] Haldeman, C., and Dunn, M., 2004, "Heat-Transfer Measurements and Predictions for the Vane and Blade of a Rotating High-Pressure Turbine Stage," *ASME J. Turbomach.*, **126**, pp. 101–109.
- [14] Povey, T., Chana, K., Jones, T., and Hurriion, J., 2005, "The Effect of Hot-Streaks on HP Vane Surface and Endwall Heat Transfer: An Experimental and Numerical Study," ASME Paper No. GT2005-69066.
- [15] Nicklas, M., 2001, "Film-Cooled Turbine Endwall in a Transonic Flow Field: Part II-Heat Transfer and Film-Cooling Effectiveness Measurements," ASME Paper No. 2001-GT-0146.
- [16] Graziani, R., Blair, M., Taylor, J., and Mayle, R., 1980, "An Experimental Study of Endwall and Airfoil Surface Heat Transfer in a Large Scale Turbine Blade Cascade," *ASME J. Eng. Power*, **102**, pp. 257–267.
- [17] Haldeman, C. W., Dunn, M. G., MacArthur, C. D., and Murawski, C. G., 1992, "The USAF Advanced Turbine Aerothermal Research Rig (ATARR)," *NATO AGARD Propulsion and Energetics Panel Conference Proceedings*, Vol. 527, Antalya, Turkey.
- [18] Barringer, M. D., Thole, K. A., and Polanka, M. D., 2007, "Experimental Evaluation of an Inlet Profile Generator for High-Pressure Turbine Tests," *ASME J. Turbomach.*, **129**(2), pp. 382–393.
- [19] Jones, T. V., 1995, "The Thin Film Heat Transfer Gauge-A History and New Developments," *Proc. Inst. Mech. Eng., Part C: J. Mech. Eng. Sci.*, **209**(C510), pp. 150–160.
- [20] Moffat, R. J., 1982, "Contributions to the Theory of a Single-Sample Uncertainty Analysis," *ASME J. Fluids Eng.*, **104**, pp. 250–260.
- [21] Kang, M., and Thole, K. A., 2000, "Flowfield Measurements in the Endwall Region of a Stator Vane," *ASME J. Turbomach.*, **122**, pp. 458–466.
- [22] Barringer, M. D., Thole, K. A., and Polanka, M. D., 2009, "Effects of Combustor Exit Profiles on Vane Aerodynamic Loading and Heat Transfer in a High Pressure Turbine," *ASME J. Turbomach.*, **131**(2), p. 021008.